Proc. of SPIE Vol. 2542, Optomechanical and Precision Instrument Design, ed. A E Hatheway (Sep 1995) Copyright SPIE

CONTACT STRESSES AND THEIR OPTICAL EFFECTS IN BICONVEX OPTICAL ELEMENTS

Kevin A. Sawyer
NASA Ames Research Center
Moffett Field, CA. 94035-1000

ABSTRACT

Stress analyses by the finite element and theory of elasticity methods are used to predict the stress fields and intensities in biconvex lenses subject to the contact forces of mounting. In particular, the effects of contact stresses produced by retainer rings are investigated. Typical retainer ring geometries are utilized in the study.

Stress distribution data are related to the stress birefringent characteristics of glass, and the effects of mounting forces on the performance of optical elements are predicted. Optical retardation due to stress birefringence as a function of lens radius is presented in graphical form.

Results of the numerical analyses are verified by the photoelastic method. Effects on lenses using typical mounting methods are investigated and compared to the analytic predictions. Experimental results correlate well with the analytical predictions. Results of this research indicate that properly designed and constructed retainer ring mounts produce localized stress birefringence effects which occur only in the area of contact.

Keywords: Lens mounting, Retainer rings, Stress birefringence

1.0 INTRODUCTION

An optical system functions correctly when the optical elements are mounted such that they remain in their specified positions and are not subjected to excessive mechanical deformations or stress. To achieve this goal the lens cell and barrel must be designed to withstand a range of vibration, shock, and thermal loadings that may be encountered during the service life. A well designed lens cell maintains lens centration and element spacing over the entire operating range without degradation or failure of the optics.

Typical retainer ring configurations are shown in Figure 1.[1] The sharp-edged retainer ring shown in the upper left of the figure is the classical method of mounting a lens (Figure 1A). A variation on this design incorporates an annular flexure and is shown in the lower right (Figure 1D). In this case the flexure deforms elastically under load prohibiting the generation of excessive contact stresses. Sharp-edged rings provide an advantage in that the annulus of contact and lens spacing may be controlled to a high degree of precision.[2] Also shown in Figure 1 are the tangent-edged and toroidal retainer rings. These geometries were designed with the specific intent of minimizing stress at the lens-to-retainer ring interface.

The presence of excessive stress in a lens is known to produce birefringence effects that may adversely affect optical performance. Stress birefringence, or the photoelastic effect, is the phenomenon in which the index of refraction of an optically isotropic material changes as the result of an applied stress. The presence of stress birefringence not only results in general image degradation, but also perturbs the polarization of the incident wave front. In the presence of stress birefringence, the lens may be modeled as a spatially varying linear phase retarder. [3] Consideration of this phenomenon is essential in the complete evaluation of a high performance optical system.

Standard practice when analyzing stress birefringence effects is to calculate the maximum stress level and apply the scalar retardation equation for the optical path difference (OPD).[1]

$$OPD = K * T * S \quad (1)$$

where

K = Stress optic coefficient, T = Specimen Thickness, and S = Maximum Stress Level.

This research addresses the analysis of stress fields and their optical effects that are produced by forces exerted on the lens by various retainer ring geometries. It is assumed that the maximum load on the lens is known and that the stress fields and levels within the lens are to be predicted for use in a birefringence analysis. From a purely mechanical point of view, only the stresses that may either fracture or deform the lens are of interest, and these quantities may be estimated from closed form

analytical solutions.[2] From an optical perspective, determination of the effect of the stress on the optical performance is a more elusive task as the three dimensional stress field at every point in the lens must be determined. Once the stress field is obtained, the stress-optic law is applied and the effect on optical performance is determined.

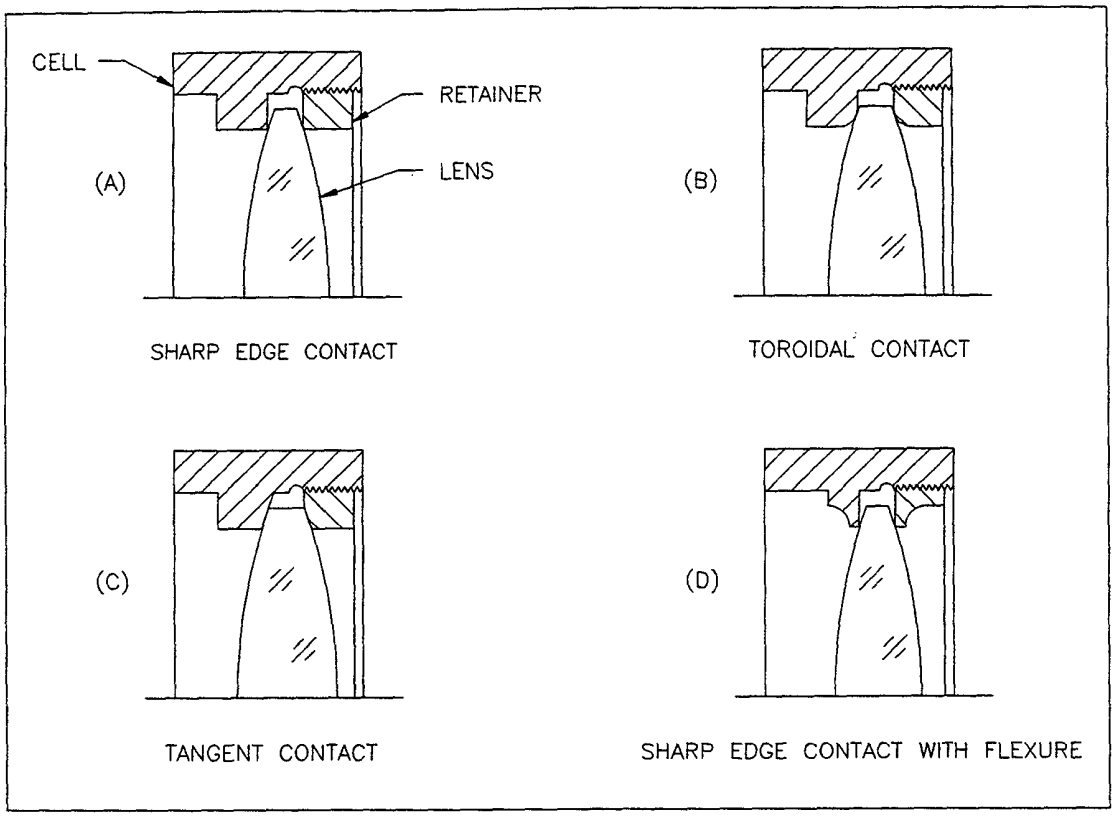

Figure 1 Typical Retainer Ring Configurations

2.0 State of stress and the stress optic effect

The tensor for a general state of stress in polar coordinates at any point in a body is given in equation 2A. At any point there exist three perpendicular planes for which all the shear terms vanish and only the normal components remain. These three normal stresses are referred to as the principal stresses, the tensor for which is shown in equation 2B. The principal stress state is determined from the general case by means of three dimensional transformation.

$$\begin{bmatrix} \sigma_{rr} & \tau_{r\theta} & \tau_{rz} \\ \tau_{\theta r} & \sigma_{\theta\theta} & \tau_{\theta z} \\ \tau_{zr} & \tau_{z\theta} & \sigma_{zz} \end{bmatrix} \quad (2A)$$

$$\begin{bmatrix} \sigma_{11} & 0 & 0 \\ 0 & \sigma_{22} & 0 \\ 0 & 0 & \sigma_{33} \end{bmatrix} \quad (2B)$$

A graphical representation of this transformation is shown in Figure 2 and is referred to as Lame's stress ellipsoid. The semi-axes of the ellipsoid give the principal stresses and the surface defines a domain of all possible states of stress at the point. Secondary principal stresses, $\sigma 1$ and $\sigma 2$, may be defined for any value of σzz that lies on the z axis. This concept is illustrated in Figure 3.

A retainer ring making full annular contact with a convex lens produces an axisymmetric state of stress in the lens. Letting the z-axis be the optical axis of the lens, the stress tensor for this state of stress is given in equation (3), where r and θ are the radial and tangential directions. The σzz term is due mainly to the Hertz compressive stresses and the σ_{rr} and σθθ components are a result of the Poisson effect due to the applied Hertzian line load.

$$\begin{bmatrix} \sigma_{rr} & 0 & \tau_{rz} \\ 0 & \sigma_{\theta\theta} & 0 \\ \tau_{zr} & 0 & \sigma_{zz} \end{bmatrix} \quad (3) \qquad \begin{bmatrix} \sigma_1 & 0 & \tau_{1z} \\ 0 & \sigma_2 & 0 \\ \tau_{z1} & 0 & \sigma_{zz} \end{bmatrix} \quad (4)$$

Utilizing the concept of secondary principal stresses, the axisymmetric stress tensor may be represented as in equation (4). Here σ1 and σ2 are the secondary principal stresses and are perpendicular to the propagation of the light ray while the normal and shear components, σzz and τz1, are parallel to the direction of propagation.

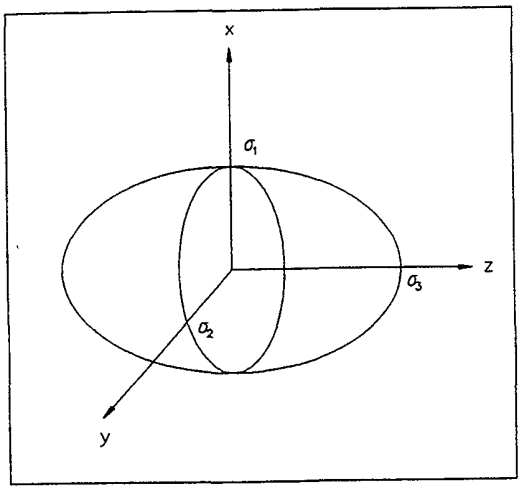

Figure 2 Lame's Stress Ellipsiod

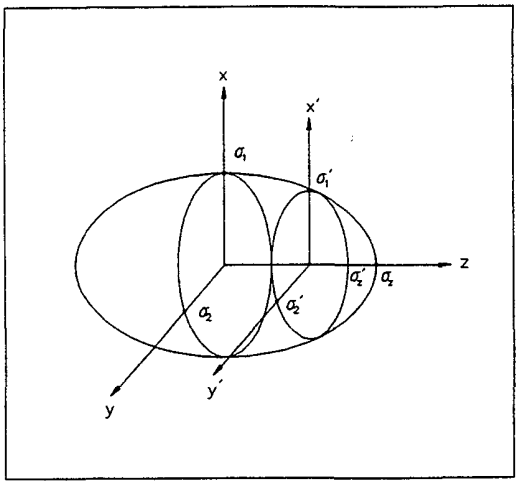

Figure 3 Secondary Principal Stresses

For a stress birefringent material the stress optic law relates the state of stress at a point to the index of refraction. The classic form of the stress optic law is

$$n_1 - n_2 = C(\sigma_1 - \sigma_2) \qquad n_1 - n_3 = C(\sigma_1 - \sigma_3) \qquad n_2 - n_3 = C(\sigma_2 - \sigma_3). \quad (5)$$

where n1, n2 and n3 are the principal indices of refraction, C is the stress optic coefficient and σ1, σ2, and σ3 are the principal stresses at a point.

The indices of refraction for an anisotropic crystal may be represented in a form similar to that of Lame's ellipsoid. This construction is known as the Index Ellipsoid for a crystal and is shown in Figure 4. The stress optic relationship is depicted in Figure 5 and demonstrates the linear relationship between the principal stresses and indices of refraction. This relationship allows for the determination of the indices of refraction at any point once the stress state is known.

A more useful form derived by Yiu and Meyer [4] gives the change of index at a point as a function of the nominal index n_0, the stress optic coefficient C, and the difference of the secondary principal stresses σ1 and σ2.

$$\Delta n = -0.5 * n_0^3 * [\, C * (\sigma_1 - \sigma_2)] \quad \text{or;} \qquad \Delta n = -0.5 * n_0^3 * [\, C * \tau_{12}] \quad (6)$$

It is significant that only the stress components perpendicular to the direction of light propagation affect the index of refraction for that particular ray of light. The z component, which is the Hertz compressive stress has no effect on the propagation of the ray.

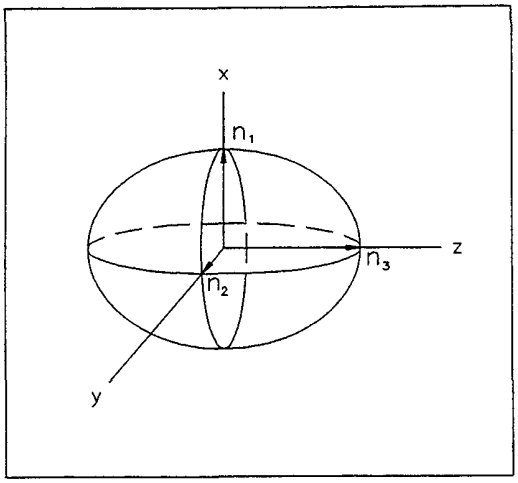

Figure 4 Index Ellipsoid

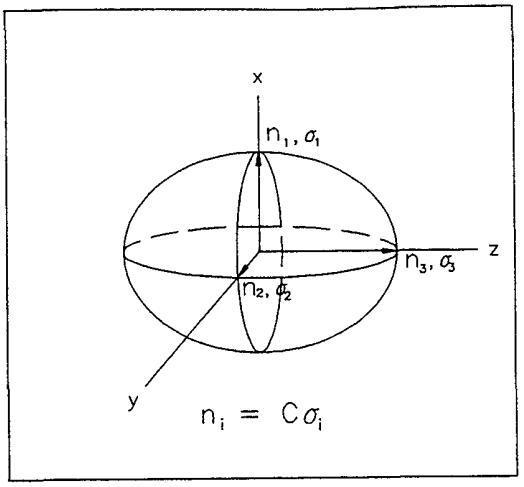

Figure 5 Stress Optic Relationship

This result is used to calculate the optical retardation in a stress birefringent material due an applied stress. For a specimen subject to a uniform stress field, of thickness t and light of wavelength λ, and Δn from equation (6), the optical retardation in units of waves is,

$$\delta = \frac{\Delta n * t}{\lambda} \tag{7}$$

3.0 Calculation of the Stress and Stress Birefringence in the Lens

Estimated values of the contact stress levels in a lens due to retainer ring mounting forces are obtained by modeling the lens and retainer as two cylinders in contact in the appropriate Hertz formulae [2]. These well-known equations give the contact width b, the maximum compressive stress P_{max}, and the maximum subsurface shear τ_{max} [5]. They are, respectively;

$$b = \sqrt{\frac{4 * p * r}{\pi * E}} \qquad P_{max} = \sqrt{\frac{p * E}{\pi * R}} \qquad \tau_{max} = 0.3\, P_{max} \tag{8}$$

where;

$$E = \frac{1}{\left(\frac{1-v_1^2}{E_1} + \frac{1-v_2^2}{E_2}\right)} \qquad \text{and} \qquad R = \frac{1}{\left(\frac{1}{R_1} + \frac{1}{R_2}\right)}$$

and the subscripts 1 and 2 represent the properties for the lens and retainer rings respectively. E is Young's modulus and R1 and R2 are the radii of curvature of the two surfaces in contact.

In order to determine the geometry and magnitude of the stress field present in a retainer-ring mounted lens, the finite element method was used. For this study, axisymmetric finite element models similar to the one shown in figure 6 were generated. The stress on each element could then be determined and the above optical retardation equation were used to determine each element's retardation contribution. The individual retardations are then summed along a path through the lens at each z coordinate. This process is depicted in Figure 7. At any radius R, there are i elements through the thickness of the lens. Since an axisymmetric state of stress is assumed there is no θ dependence.

The load distributions for the finite element models are shown in figure 8. The sharp edged ring is simulated by a point load on the model. The toroidal and tangent ring loads are simulated by distributing the loads to roughly resemble a Hertz stress distribution which is parabolic in shape. This method of applying line loads to the finite element models was validated by Shih and Schlein [6] who demonstrated that the stress fields outside of the immediate area of contact produced by these loadings are accurate and correlate with experimental results.

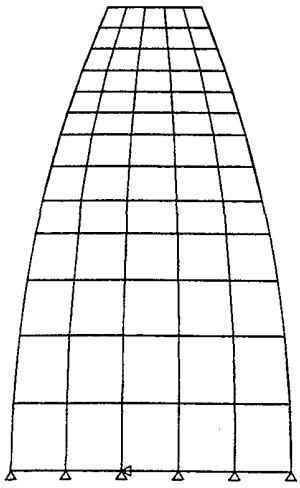

Figure 6 Finite Element Model

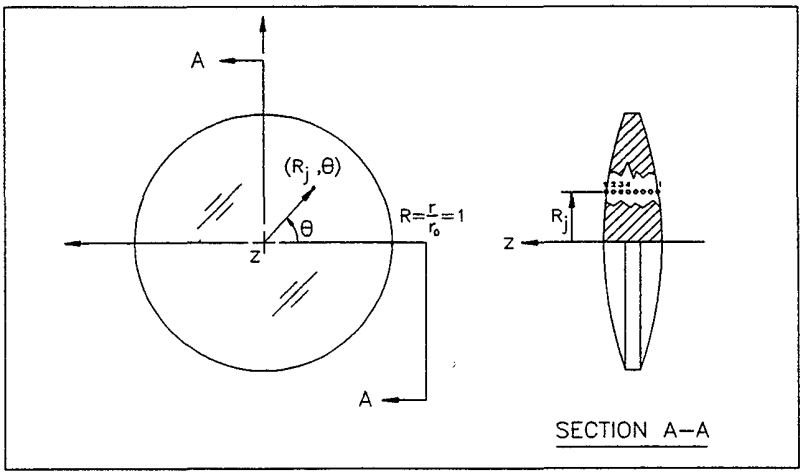

Figure 7 Calculation Of The OPD Through The Lens

Presented in section 4.0 are the results from four finite element models of lenses with f/#'s ranging from 1.5 to 4. Each model was run with each of the three retainer ring loads. The nodal stress and model geometry data from the finite element analysis were retrieved and used in specially developed FORTRAN programs that calculate the stress birefringence present in the lens [7]. Lens clamping forces were calculated from the equations developed by Yoder[1] and are representative of preloads required for MIL-SPEC survivability. These preload forces are equal to approximately 100 pounds of axial preload per cubic inch of glass.

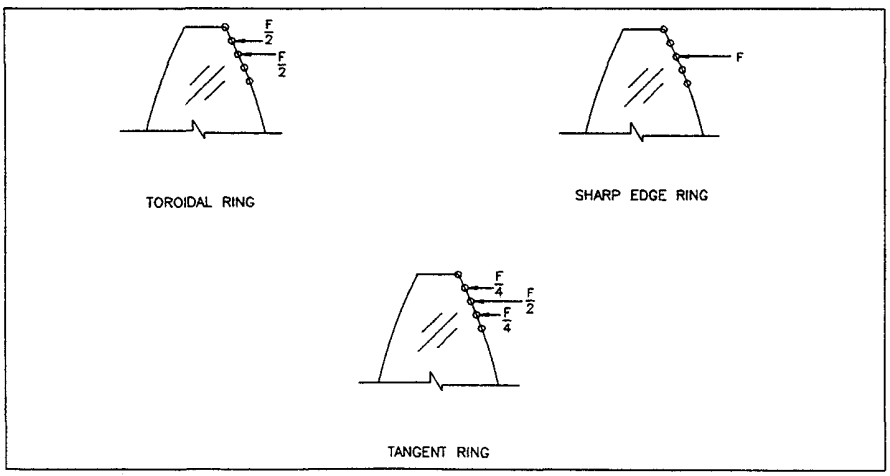

Figure 8 Finite Element Load Distributions

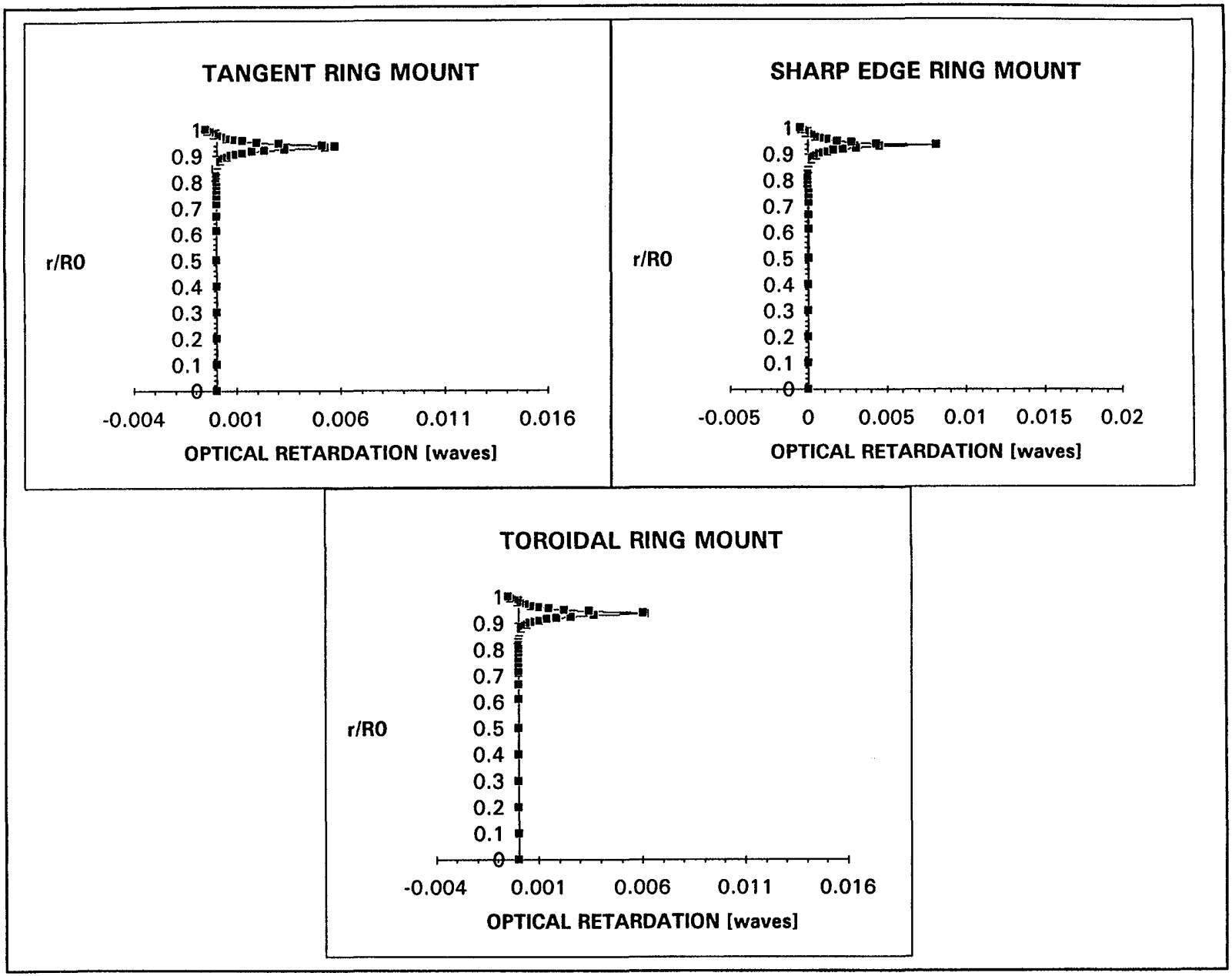

Figure #9 OPD Plots for f/5 Lens

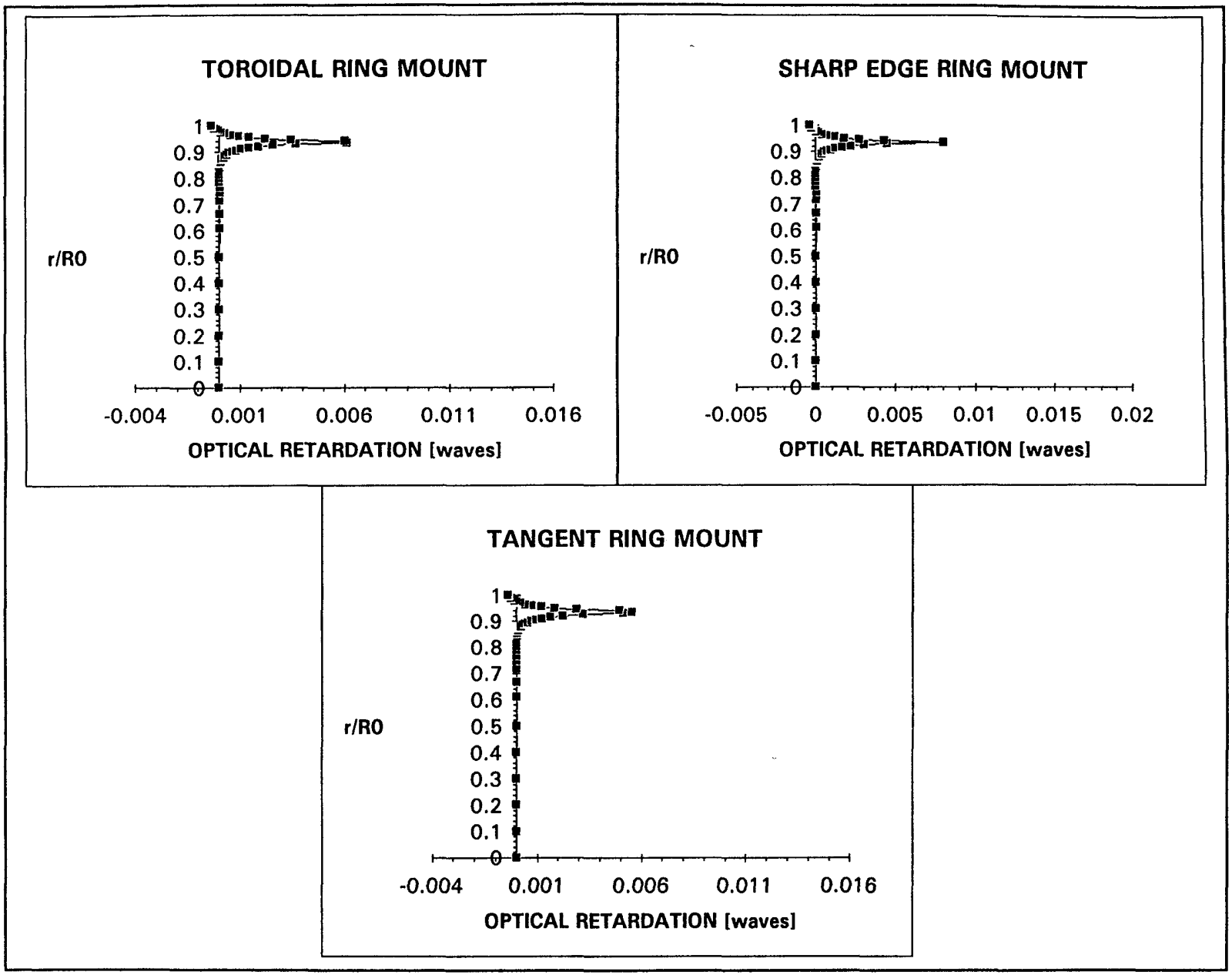

Figure #10 OPD Plots for f/4 Lens

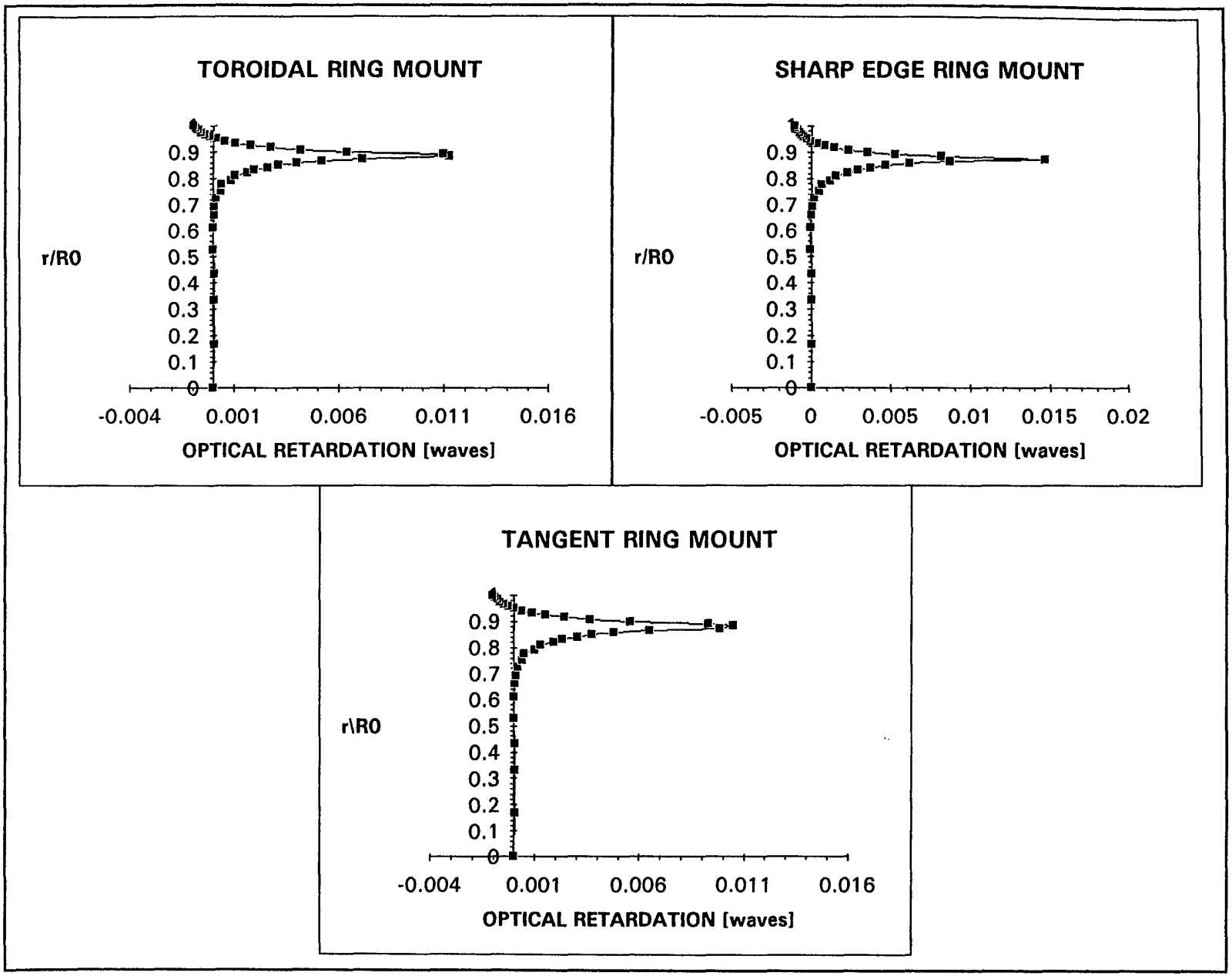

Figure #11 OPD Plots for f/2.5 Lens

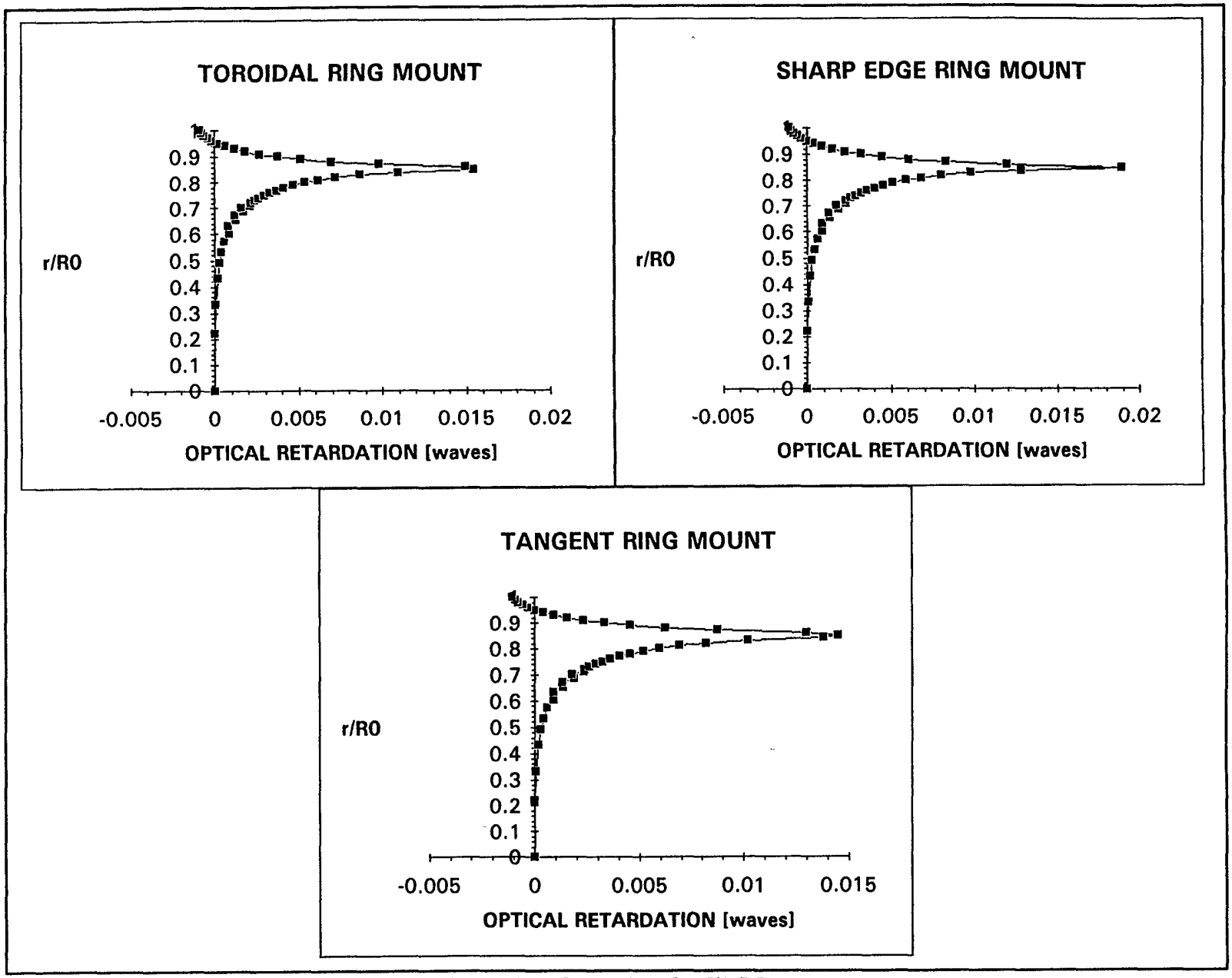

Figure #12 OPD Plots for f/1.5 Lens

4.0 Calculation of the Field dependent retardations.

The OPD graphs shown in figures 9 through 12 for the retainer ring assemblies indicate that there should theoretically be little difference in the performance of the three mounts. In none of the cases is the level of stress birefringence in the clear aperture of the lens greater than 0.01 waves. The amount by which the stress birefringence extends into the clear aperture of the lens is affected only slightly by varying the ring geometry. The peak value of retardation for all lenses is highest for the sharp edge ring. An edge effect is apparent outside of the annulus of contact. Here the radial stress approaches zero near the boundary and the tangential stress term dominates in the OPD expression, thereby resulting in a change in sign of the calculated OPD near the edge of the lens

The extent of the birefringence field is directly dependent upon the lens curvature with the low f/# lenses having more stress birefringence than the high f/# lenses. This dependence on lens curvature results from the axially applied clamping forces being applied to a curved surface. Since the clamping force is applied parallel to the axis of symmetry, both normal and tangential components are present at the point of contact. As the curvature of the lens surface increases so does the angle of the normal force with respect to the axis of symmetry. This rotates the contact stress field toward the center of the lens. Figure 13 shows how the contours of constant subsurface shear are effected by this rotation. This model is substantiated by the finite element stress data which demonstrate the asymmetry of the stress field about the point of contact for steeply curved lenses.

A significant result of the retainer ring analysis is that the stress birefringence is highly localized in all cases. Additionally, the result contradicts the idea that sharp-edged retainer rings produce a greater amount of stress birefringence than toroidal or tangent-edged contacts. The correct observation is that, although sharp edged rings produce greater local contact stress effects, the global effects produced are equivalent to those of toroidal or tangent rings.

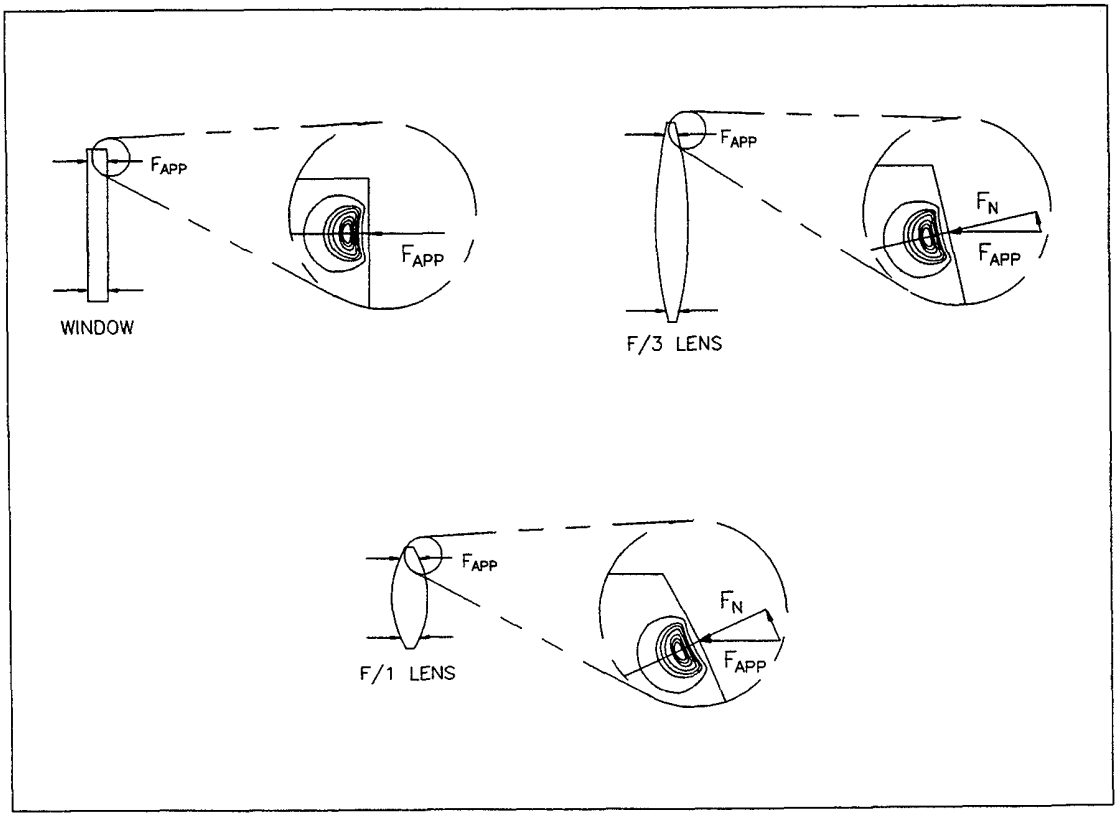

Figure 13 Rotation of the Contact Stress Field

5.0 Experimental Results

To verify the analytical results, a photoelastic experiment was designed and performed. The apparatus consists of a circular polariscope with Tardy compensation, an immersion cell, a universal lens mount with interchangeable retainer rings, a torque wrench, a 35mm camera with macro lens, and six glass lenses with f/#'s from 1.5 to 5.

The universal lens cell is shown in figure 14. The interchangeable retainer rings are keyed in the housing to prevent rotation during torquing of the compression nut. Retainer ring configurations as shown in figure 1 were designed for each lens. All parts were fabricated in an in house machine shop using standard tolerances and machining practices.

For the experiment, each lens was assembled in each of the four retainer ring configurations and axially preloaded to give 100 pounds of force per cubic inch of glass. The preload was obtained using the torque wrench for tightening the compression nut to a torque obtained from the equation, $T = 0.2*F*D^3$. Where F is the required axial preload and D is the thread diameter of the nut. All assemblies were observed through the polariscope using standard photoelastic analysis procedures[8].

For lenses with f/#'s greater than 2, no birefringence effects were observed in any sharp-edged retainer ring assembly. For f/#'s less than 2, the sharp-edged ring produced a faint annular zone of birefringence occurring near the ring of contact. This is not an unexpected result due to the inability of the finite element analysis to accurately predict the stresses in the immediate region of contact. These results are consistent with the analytical predictions in figures 9 through 12.

Birefringence effects were observed in a number of the toroidal and tangent edged retainer ring assemblies. These fields were irregular in nature and were attributed to machining irregularities on the interface surface making a series of point contacts with the lens. The rigid nature of these rings does not allow a complete annular contact to form as in the case of the flexured sharp-edged ring which produced no birefringence during any of the experimental trials.

The experiment demonstrated the need for accurate fabrication and assembly of the lens cell components in order to achieve predictable behavior of the birefringence fields. Lenses that were not centered prior to assembly often became pinched along a sector and exhibited excessive localized birefringence. In all cases this problem was rectified by reassemble of the components. This problem became much less frequent as assembly experience increased. Excessive local birefringence also occurred when the retainer rings were not made to specification and had burrs or irregularities in flatness in the area of contact with the lens. This phenomenon was entirely predictable by careful inspection of the retainer rings prior to assembly.

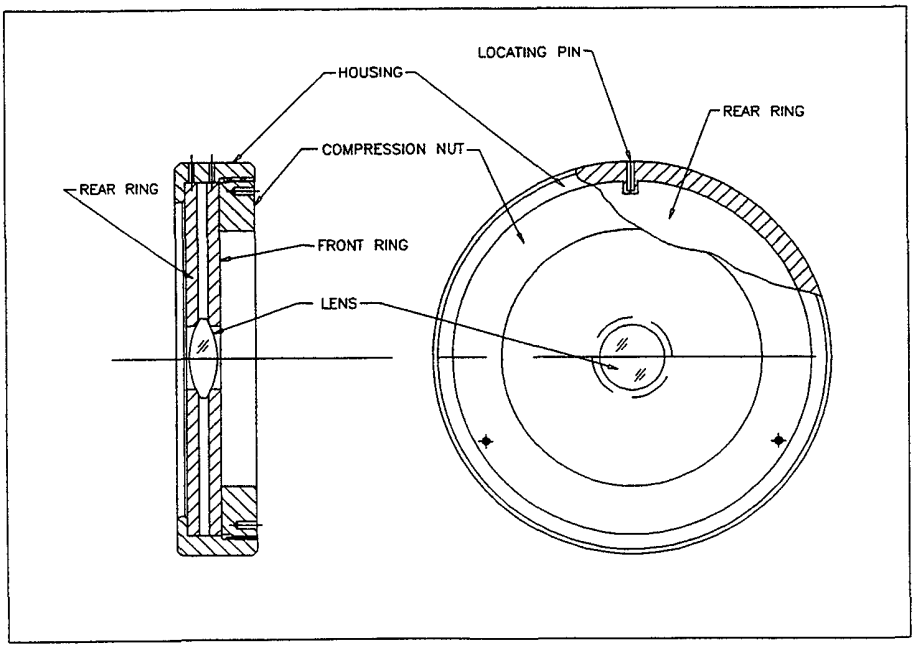

Figure 14 Universal Lens Cell With Interchangeable Retainer Rings

6.0 Discussion and Conclusions

The stress fields and associated birefringence effects for retainer ring mounted lenses have been successfully predicted by the finite element method. The analytic results are presented in graphical form for ease of interpretation. Furthermore, the analytic predictions were verified by photoelastic analysis and demonstrated a high degree of correlation.

The sharp-edged retainer ring has proven to be an excellent mount for the minimization of stress birefringence. Although the Hertz stresses are apparently high at the annulus of contact, the stress field is localized and diminishes rapidly. The sharp-edged rings also have the best self aligning and centering characteristics and are the easiest to assemble in an accurate fashion. It is noteworthy that during all the experimental trials, even at compression nut torque in excess of 800 in-lbf, not a single lens fractured during assembly.

The toroidal and tangent-edged rings, while minimizing the Hertz stresses at the point of contact, produced larger stress fields than the sharp-edged rings. Thus, the intensity of the birefringence was reduced at the cost of extending its region of influence. These rings also have a reduced self centering tendency during assembly and greater care and skill is required not to pinch the lens out of center. The sensitivity to machining errors is also greater for these geometries. Small burrs or waves in the contact surface tend to print through onto the lens producing regions of localized birefringence in the lens.

The method developed during this research allows for accurate prediction of birefringence effects in lenses mounted with retainer rings. The optimal retainer ring configuration proved to be the flexured sharp-edged. This geometry gave predictable birefringence free performance in all experimental trials. The rigid sharp-edged ring also provides predictable performance, however in some cases produces limited birefringence effects in a thin annular zone about the perimeter of the lens. The toroidal and tangent edged rings produced varied results. Lenses mounted with these types of rings were prone to exhibit birefringence fields resulting from assembly or machining errors. The uncertainties involved in manufacturing and assembling these types of rings dictate that the optic be checked for birefringence after assembly.

References

1. Yoder, Paul R., *Opto-Mechanical Systems Design 2nd edition*, Dekker 1992.

2. Delgado and Hallinan, *Mounting of Lens Elements*, Applied Optics, Vol. 14, No 1, 1975.

3. Theocaris, P. S. and Gdoutos, E. E., *Matrix Theory of Photoelasticity*, Springer-Verlag, 1979.

4. Yiu, Y. C. and Meyer, A. R., *Computation of Optical Errors in Transparent Optical Elements due to Three Dimensional Photoelastic Effect*, Proceedings of SPIE - the International Society for Optical Engineering, Vol. 1303, 1990.

5. Johnson, K. L., *Contact Mechanics*, Cambridge University Press, 1985.

6. Shih and Schlein, *Photoelastic and Finite Element analysis of different size spheres in contact*, J. Mater. Res., Vol. 7, No 4, 1992.

7. Sawyer, K. A. *Contact stresses and their optical effects in biconvex optical elements.*, The University of Arizona, 1995.

8. Dally, J. W. and Riley, W. F., *Experimental Stress Analysis*, McGraw-Hill, 1978.